24th INTERNATIONAL CONGRESS ON SOUND AND VIBRATION
23–27 July 2017, London

ICSV24
23-27JULY 2017
LONDON CALLING

ACOUSTIC CORRECTIONS FOR A KEVLAR WALL WIND TUNNEL USING A PULSED-LASER POINT SOURCE

Kyle Pascioni, Andrew Colangelo, Louis Cattafesta
Florida State University, Department of Mechanical Engineering, Tallahassee, FL, USA
email: lcattafesta@fsu.edu

The use of Kevlar sidewalls in an anechoic wind tunnel facility is becoming a popular technique for aeroacoustic measurements. In many circumstances, aerodynamic properties can more closely approximate free-air boundary conditions relative to an open jet while still allowing acoustic information to pass for far field observation. However, the imposition of this test section environment has not been fully addressed. To understand the necessary data corrections, a non-intrusive source is used for acoustic characterization. The beam from a pulsed laser is focused to generate a plasma point source, where the byproduct is a spherically spreading pressure impulse. This source type proves useful to overcome the additive flow-noise associated with positioning a speaker housing in the flow, while providing a source rich in frequency content. Through the use of frequency response functions between data acquired in various tunnel configurations, the frequency dependent no-flow transmission loss is found and compared with acoustic theory. The influence of the Kevlar wall boundary layer is also estimated. This information is gathered on a per microphone basis, allowing direct application of magnitude and phase corrections for single microphone signals or array based methods.

Keywords: Aeroacoustics, Wind Tunnel Corrections, Kevlar

1. Introduction

Aeroacoustic measurements are typically performed in an open-jet test section given their close representation of a free field acoustic environment. Problems can arise, however, when studying lifting bodies. The jet boundary permits streamline curvature, altering the mean aerodynamic conditions relative to an 'infinite' free stream found in actual flight. To first order, a large angle of attack correction can be used to counter the open-jet effect. While integrated aerodynamic forces can typically be matched, equivalent surface pressure distributions often cannot be realized. Moreover, tunnel jet deflection can increase background noise levels due to flow recirculation in the anechoic chamber. The former decreases signal-to-noise ratio, and the latter can increase hydrodynamic self-noise on the microphones. While good aerodynamic characteristics are typically obtained using conventional hard wall test sections, the rigid wall produces a reverberant acoustic environment.

To marry the acoustic benefits of the open-jet and the aerodynamic benefits of a hard wall test section, a fairly new approach involving the use of Kevlar sidewalls has been implemented in the Florida State Aeroacoustic Tunnel based on the work of [1]. Porous Kevlar walls are positioned at the test section boundaries and tensioned for increased rigidity. The wall bounds the flow similar to a conventional rigid-wall tunnel, but is thin enough to allow acoustic waves to pass with minimal transmission loss. The sidewall material used here is plain weave Kevlar 49, 195 denier (also referred to as Type 120) fabric. This material is chosen due to a number of previous findings, one of the first being by [2], who found minimal transmission loss relative to several other materials. They used this

method in an attempt to reduce self-noise on a recessed acoustic array in a hard wall wind tunnel, and is still used today by others [3]. It was then Devenport et. al [1] and subsequently Ito et. al [4] extrapolated this idea to the test section walls in an effort to retrofit their conventional tunnels for aeroacoustic measurements.

As mentioned above, the Kevlar material has a small impact on the propagating acoustic field prior to being measured in the far field. However, the losses can be important, especially at high frequencies as the wavelength approaches the wall thickness. To date, corrections are in the form of frequency dependent transmission loss [5, 1], typically found using a broadband calibration speaker. Here, a pulsed-laser, first introduced by Bahr et. al [6], is used as the calibration source given its ability to generate a non-intrusive impulsive point source. Current techniques are limited to correcting the sound pressure level neglecting important phase differences which may be present. Beamforming with microphone arrays can thus be greatly affected due to the Kevlar wall itself and refraction and scattering of the waves as they pass through the wall boundary layer. The result is an unknown loss of accuracy in beamforming results.

The aims of this article are twofold: (1) to understand the relative importance of the wall versus the boundary layer acoustic loss mechanisms and (2) to present an effective correction method for general use. The experimental method is described, along with a description of the laser-pulse point source and processing methodology using frequency response functions. Normal incidence acoustic theory without flow is used to calculate the transmission loss of the Kevlar material and is compared to experimental results. Then, with the addition of flow, the effects of the Kevlar wall boundary layer is examined.

2. Experimental Setup and Methods

The wind tunnel facility and instrumentation will first be discussed in this section. A description of the calibration source will then be presented, followed by an outline of the frequency response function method to obtain the desired corrections.

2.1 Facility and Instrumentation

The experiments are performed in the Florida State Aeroacoustic Tunnel (FSAT) [7]. Flow speeds up to 75 m/s (approximately Mach 0.2) can be obtained in the test section, which measures 1.219 $\times$ 0.914 $\times$ 3.05 m (spanwise $\times$ vertical $\times$ streamwise). Surrounded by a 250 Hz anechoic chamber, the test section is outfitted with two Kevlar sidewalls tensioned to approximately 15 N/cm while the floor and ceiling are acrylic to accommodate optical flow diagnostics.

The acoustic microphone array is located in a sideline position in the anechoic chamber outside of the flow 1.2 m away from the test section center. Consisting of 55 channels, the relative microphone locations are optimized over a frequency range of 1-16 kHz based on the principles outlined by [8]. A combination of 1/4-inch G.R.A.S. 40BE and Brüel and Kjær 4958 free field microphones populate the array. An aluminum skeletal frame is used and treated with foam wedges to minimize acoustic reflection and scattering. For brevity, the reader is referred to [9] for additional details of the array.

The microphone signals are digitally acquired using National Instruments hardware (NI-4462 and NI-4498 cards in a NI-PXI-1045 chassis). Additionally, a photodiode (Scitech Inc, Type 301-020) is simultaneously sampled to identify the instance of each laser pulse for post-processing.

2.2 Acoustic Source

The chosen source is a repetitive acoustic impulse formed by focusing a high-energy laser beam to a point, similar to that described by [6]. They showed its potential in an open-jet aeroacoustic facility, finding results to be consistent with theory [10] for predicting both convective shifts in source location and shear layer refraction. Outside of the test section, the beam of a 200 mJ Quantel Evergreen pulsed

laser is passed through an optical lens assembly as depicted in Fig. 1. The beam is first expanded and subsequently refocused to increase the solid angle of convergence, which in turn, can minimize the spot size to maximize energy density deposition. Localized heating breaks down the air at the focus point, forming a plasma with a lifetime on the order of nanoseconds [6]. The byproduct is a spherically propagating pressure wave acting as a compact monopole-like acoustic impulse. In essence, an acoustic field with a delta function in both space and time is produced. This deterministic source type overcomes the additive random flow-noise associated with positioning a speaker in the flow, while generating a compact acoustic source rich in frequency content. Moreover, the finite lifetime of the source allows processing techniques to reveal relative effects of facility reflections. As will be shown, reflections due to the presence of the test section boundaries will be removed in the time domain when desired. To reduce random uncertainty, the laser repetition rate is set to 10 Hz and sampled for a total of 300 s, resulting in 3,000 events per case. Seeding the test section with Di-Ethyl-Hexyl-Sebacat (DEHS) improved the success rate of generating an acoustic source yielding a near 100% success rate in the absence of a free stream, and approximately 95% with flow.

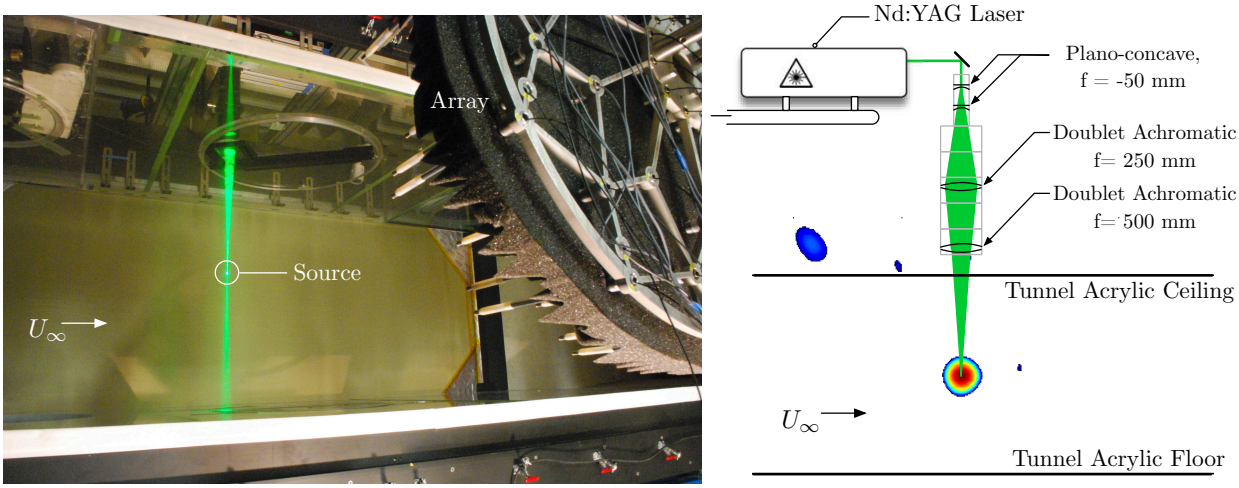

Figure 1: Image of laser pulse source setup (*left*) and schematic illustrating the laser and lens assembly with representative beam map (*right*, not to scale).

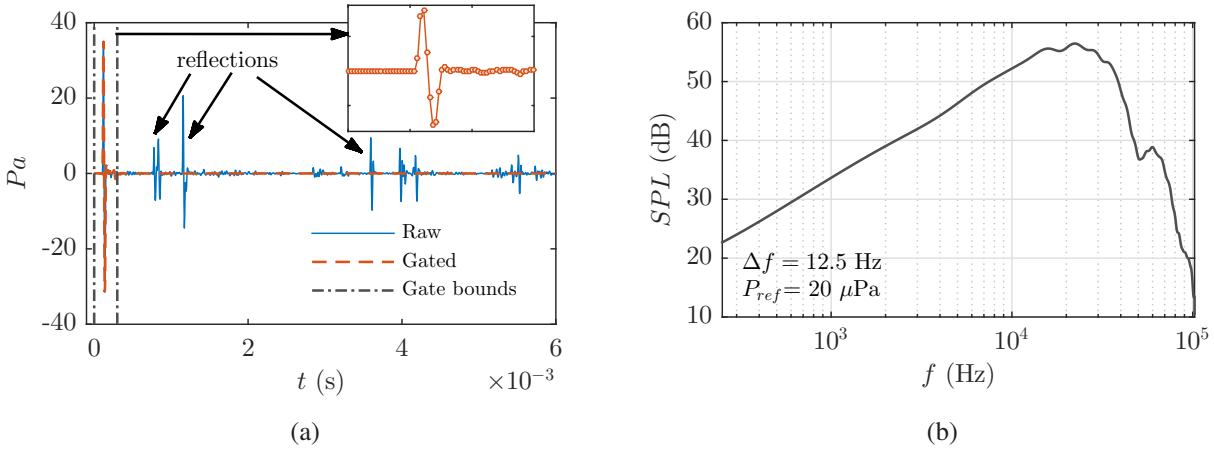

(a) (b)

Figure 2: Laser pulse signal characteristics as measured by an array microphone, illustrating (a) the raw time signal with and without gating the initial impulse. The inset figure shows the shape of the initial impulse, with the independent axis limits at the gate bounds and (b) the sound pressure spectrum of the gated signal.

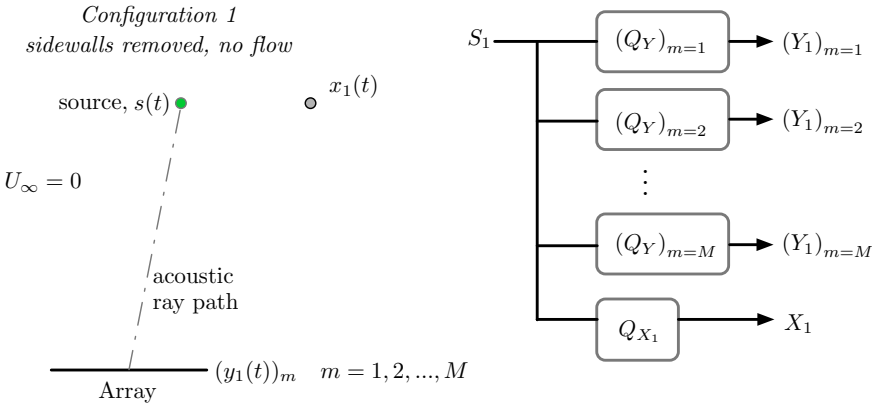

(a)

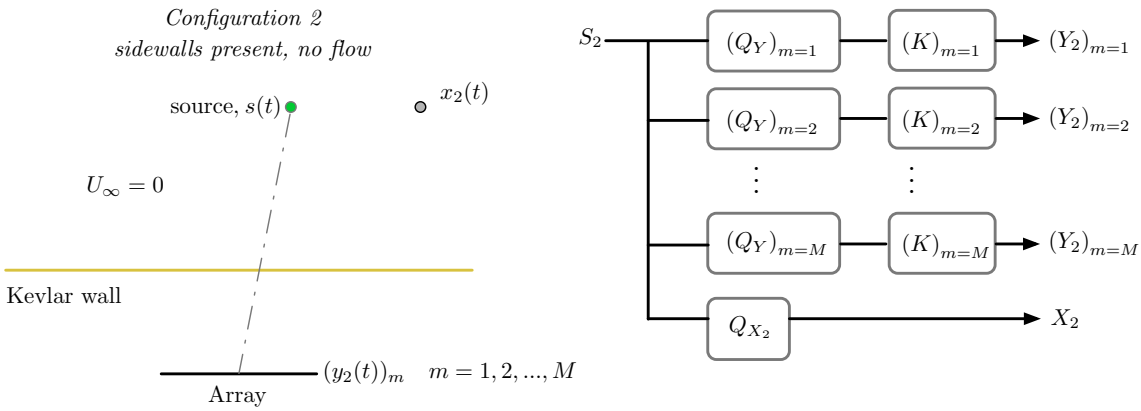

(b)

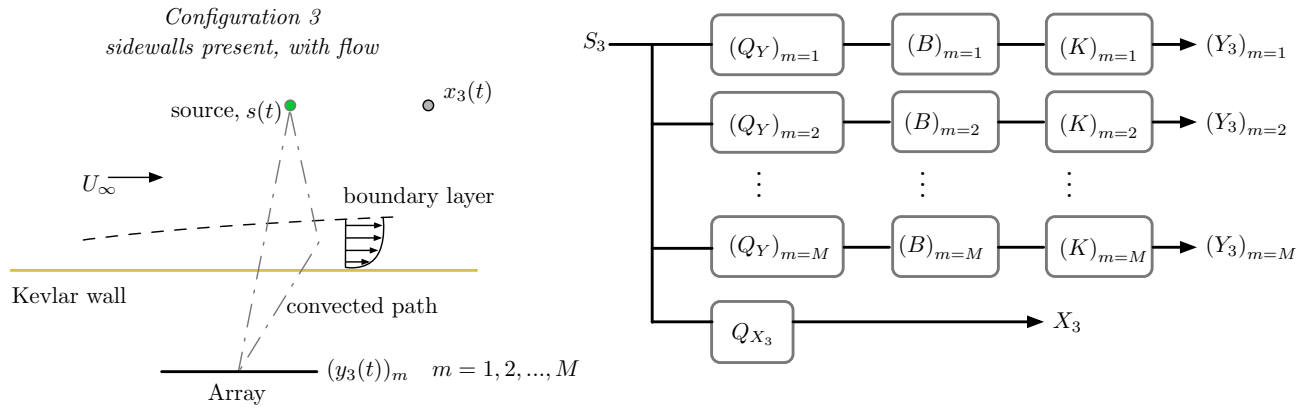

(c)

Figure 3: Schematic of the three test section configurations, (a) sidewalls removed/no flow, (b) sidewalls present/ no flow, and (c) sidewalls present/with flow, with corresponding frequency domain block diagrams. See text for notation description.

2.3 Frequency Response Function Description

A frequency response function (FRF) analysis is used to determine the Kevlar transmission loss and the effect of the Kevlar wall boundary layer. Reflections from the testing environment (sound-hard acrylic floor and ceiling, the Kevlar itself, etc.) are first removed for this analysis. To do so, the time signal is gated to retain only the direct-path-impulse, while the secondary reflected waves are removed.

An example of this processing technique from a selected array microphone is shown in Fig. 2(a). The resulting sound pressure spectrum, computed by

$$SPL = 10 \log_{10} \left(\frac{\hat{G}_{p,p} \Delta f}{P_{ref}^2} \right), \tag{1}$$

with bin width Δf, $P_{ref} = 20$ μPa, and the auto-spectral density function is estimated by ensemble averaging N_b blocks (or the number of impulse events),

$$\hat{G}_{p,p} = \frac{2}{T_b} \frac{1}{N_b} \sum_{i=1}^{N_b} [P^*(f) P(f)], \tag{2}$$

and is also given in Fig. 2(b). The hat symbol denotes an estimate of the true power spectral density, i.e.,

$$\hat{G}_{p,p} \approx G_{p,p} = \lim_{T_b \to \infty} \frac{2}{T_b} E\left[P^*(f) P(f)\right] \tag{3}$$

In these equations, $E[\cdot]$ is the expectation operator, each record has length T_b, $P(f)$ is the Fourier transform of the gated time signal $p(t)$, and $(\cdot)^*$ denotes the complex conjugate. Each data block holds one impulse event and is zero-padded to obtain a block length of 8,192 samples. The sampling frequency is 204.8 kHz, maximized for the acquisition system to resolve the short duration pressure wave, resulting in 8-9 samples during the passage of the initial impulse (see inset of Fig. 2(a)). All data presented henceforth will retain the same processing parameters.

Three test section configurations are used as depicted in Fig. 3 and modeled using appropriate block diagrams. For each configuration i, $(Y_i)_m$ and X_i represent the measured array signal of microphone m and the reference signal, respectively. The reference microphone is mounted in the flow to a 15.2 cm chord NACA 0012 airfoil strut 0.5 m downstream of the source location. This was deemed necessary due to the fact that each pulse must be measured prior to passing through the Kevlar or boundary layer due to slight shot-to-shot variations in the pulse amplitude. A Brüel and Kjær nose cone (Type UA-0385) is installed on the inflow microphone to minimize hydrodynamic contamination of the reference. Source S represents the laser-generated acoustic impulse where $(Q_Y)_m$ accounts for acoustic propagation from the source to array microphone m, while Q_{X_i} accounts for acoustic propagation from the source to the reference microphone. When the Kevlar wall is present, an additional block K describing the frequency dependent transmission loss is required. When a non-zero free stream flow is added, B accounts for the resulting difference in the measured array signals by the boundary layer. Had the signals not been gated, an additional block would be necessary to account for reflections. These block diagrams will be used to generate the FRFs that enable estimation of the transmission loss K and effect of the boundary layer B. The following sections will apply this methodology.

3. Results

This section begins by determining the no-flow Kevlar transmission loss, along with comparison with normal incidence acoustic theory. Boundary layer effects will then be found using a similar approach.

3.1 Kevlar Transmission Loss

Auto- and cross-spectral density functions are first computed using the measured data. On a per microphone basis (the subscript m will be momentarily suppressed), the auto-spectral density of the array signal from test section configuration 1 can be modeled using the block diagram,

$$\hat{G}_{Y_1,Y_1} = E[Y_1^* Y_1] = E[Q_{Y_1}^* S_1^* Q_{Y_1} S_1]. \tag{4}$$

The cross-spectral density function for a given microphone between configuration 1 and 2 is given as

$$\hat{G}_{Y_1,Y_2} = E[Y_1^* Y_2] = E[Q_{Y_1}^* S_1^* K Q_{Y_2} S_2]. \tag{5}$$

Note that although the data Y_1 and Y_2 are not simultaneously sampled, the photodiode signal is used to align impulse events. The reference signals are processed similarly,

$$\hat{G}_{X_1,X_1} = E[X_1^* X_1] = E[Q_{X_1}^* S_1^* Q_{X_1} S_1], \tag{6}$$

$$\hat{G}_{X_1,X_2} = E[X_1^* X_2] = E[Q_{X_1}^* S_1^* Q_{X_2} S_2]. \tag{7}$$

Finally, reinstating subscript m to denote a specific microphone, $\hat{H}_k$ which is equivalent to K can be found,

$$(\hat{H}_k)_m = \left(\frac{\hat{G}_{Y_1,Y_2}}{\hat{G}_{Y_1,Y_1}}\right)_m \frac{\hat{G}_{X_1,X_1}}{\hat{G}_{X_1,X_2}} = \frac{K_m Q_{Y_{2,m}} S_2}{Q_{Y_{1,m}} S_1} \frac{Q_{X_1} S_1}{Q_{X_2} S_2} = K_m. \tag{8}$$

The above relation holds by assuming the FRFs Q_Y and Q_X are identical between configuration 1 and 2. Note that S_1 and S_2 cancel, illustrating that the result is independent of source amplitude.

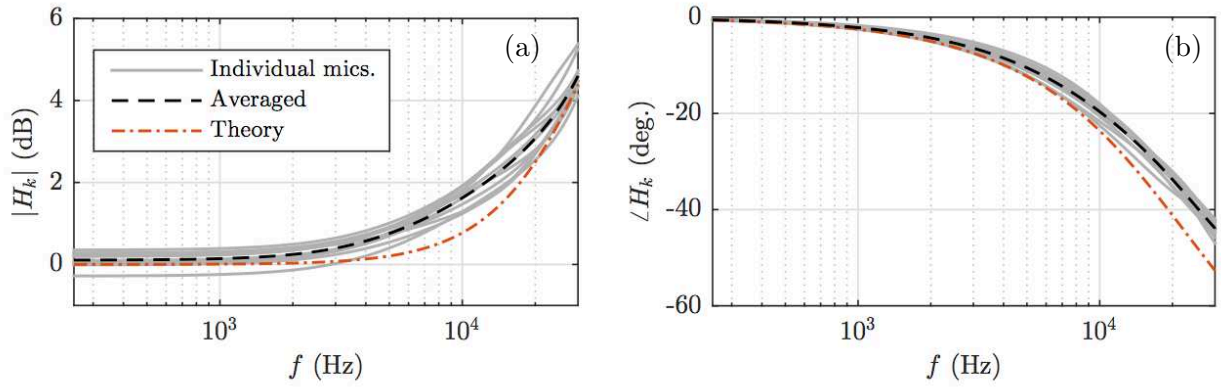

Figure 4: Magnitude and phase of FRF modeling the Kevlar transmission loss block K. Ten individual microphones are given along with their average, and compared to normal incidence acoustic theory.

A physics-based explanation can be useful to prove, to an extent, the validity of the experimental trend. Therefore, a simplified theoretical analysis of the problem is considered. Assume one dimensional time harmonic acoustic waves with normal incidence encounter a set of impedance changes. We will restrict this discussion to quiescent media and follow the derivation by [11]. The first and third medium is modeled to have properties of air, while the second medium has the material density and thickness of Kevlar, ρ_2 and l_2, respectively. Boundary conditions matching the pressure and normal acoustic particle velocity at each interface are introduced. After algebraic manipulation, the transmission coefficient is found,

$$T = \frac{2}{\left(1 + \frac{Z_1}{Z_3}\right)\cos(k_2 l) + j\left(\frac{Z_1}{Z_2} + \frac{Z_2}{Z_3}\right)\sin(k_2 l)}, \tag{9}$$

with the characteristic impedance defined by $Z_{(\cdot)} = \rho_{(\cdot)} a_{(\cdot)}$, the acoustic wavenumber $k = \omega/a$ is based on sound speed a, and $j = \sqrt{-1}$. When the thickness of medium 2 is very small, $\sin(k_2 l) \approx k_2 l$ and $\cos(k_2 l) \approx 1$. For Kevlar Type 120, $l = 8.89 \times 10^{-5}$ m, which gives $k_2 l = 1.24 \times 10^{-7}$ at $f = 20$ kHz, confirming the validity of this assumption. Equation 9 is further simplified by assuming $Z_1/Z_2 \ll 1$, and the fact that $Z_1 = Z_3$, reducing to

$$T = \frac{2}{2 + j\left(\frac{\rho_2 a_2}{\rho_3 a_3}\right)\frac{\omega}{a_2} l} = \frac{2}{2 + j\omega l \frac{\rho_2}{\rho_3 a_3}}, \tag{10}$$

which is an interesting result as it is independent of a_2. Hence, only the Kevlar material density is needed rather than its unknown characteristic impedance. The transmission loss can now be defined,

$$TL = -20\log_{10}(|T|). \tag{11}$$

As shown in Fig. 4, this analysis slightly underestimates the measurement, although the trend is consistent, and can be viewed as a lower bound in a limiting sense. The underestimation suggests additional factors are important such as oblique incidence, the weave pattern of the Kevlar (as opposed to a homogeneous membrane), other material properties, and wall tension. Future work will consider such effects.

The behavior of these trends are consistent with expectation. Low frequencies should be negligibly affected given the small thickness of the wall relative to the wavelength. Averaging over a set of microphones, $\hat{H}_k$ is found to be lower than 1 dB below 6 kHz, but found to increase to 3 dB at 20 kHz. Although the phase difference increases with frequency, the relative phase differences among microphones are found to be negligibly small. Thus, K does not largely affect results which employ processing techniques that only rely on relative delays (e.g., beamforming).

3.2 Effect of Kevlar Wall Boundary Layer

A similar approach is performed here by computing the same auto- and cross-spectral density functions on data acquired in test section configurations 2 and 3. The block diagram B can then be found using a combination of FRFs,

$$\begin{aligned}(\hat{H}_b)_m &= \left(\frac{\hat{G}_{Y_2,Y_3}}{\hat{G}_{Y_2,Y_2}}\right)_m \frac{\hat{G}_{X_2,X_2}}{\hat{G}_{X_2,X_3}} = \frac{E[S_2^* Q_{Y_2,m}^* K_m^* S_3 Q_{Y_3,m} B_m K_m]}{E[S_2^* Q_{Y_2,m}^* K_m^* S_2 Q_{Y_2,m} K_m]} \frac{E[S_2^* Q_{X_2}^* S_2 Q_{X_2}]}{E[S_2^* Q_{X_2}^* S_3 Q_{X_3}]} \\ &= \frac{Q_{Y_3,m} Q_{X_2} E[S_2^* S_3 B_m]}{Q_{Y_2,m} Q_{X_3} E[S_2^* S_3]}.\end{aligned} \tag{12}$$

Again, we note that the two propagation paths for the reference signals are equal, i.e., $Q_{X_2} = Q_{X_3}$, and are aligned in time to remove the convective shift, yielding pulse events that are synthetically simultaneous (note that the reference microphone is physically aligned with source and only offset in the streamwise direction). In order for $Q_{Y_2} = Q_{Y_3}$, the convection of the acoustic waves as they propagate to the array through the test section when $U_\infty \neq 0$ must be accounted for. Therefore, prior to computing equation 12, Q_{Y_3} is scaled by the ratio of the path lengths with and without flow. The ratio is found using the methods of [12]. Furthermore, the associated time delays due to source convection are removed to isolate the phase offsets by the boundary layer. Contrasting section 3.1, S_2 and S_3 cannot be removed from the expectation operator due to the random nature of the turbulent boundary layer. Fortunately, the large number of pulses used in the averaging process allows equation 12 to approximate the effects of B.

Figure 5 gives the result of equation 12. For flow speeds less than 30 m/s, $|\hat{H}_b|$ is found to be negligibly small. As flow speed increases, the magnitude increases and peaks at approximately 8 kHz, but still remains lower than 1 dB. Against expectations, each curve is found to drop at intermediate frequencies, while hinting at increasing at high frequencies. One possible explanation is the increase in background levels at these frequencies is due to Kevlar sidewall scrubbing. Alternatively, the location of the signal gating bounds was found to slightly change low and high frequency behavior. Hence, a sensitivity study of the trends with respect to the gating bounds should be considered. In any case, the minimum of the dip is found to increase with frequency (e.g., 26 kHz at 40 m/s, 28 kHz at 50 m/s), suggesting that this behavior is dependent on flow speed. It should be noted that the results here are facility dependent, and vary according to the characteristics of the boundary layer.

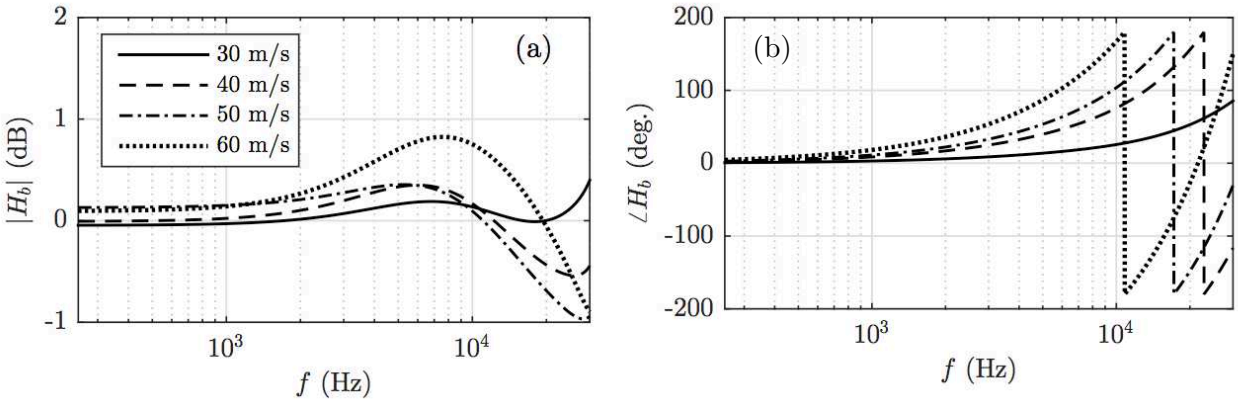

Figure 5: Magnitude and phase of FRF modeling the effect of the Kevlar wall boundary layer, B. Ten microphones are averaged in (a), while for clarity, a single representative microphone is given in (b).

4. Conclusions

A technique is described to determine the effects of the Kevlar tunnel walls to establish acoustic measurement corrections. A pulsed-laser point source provides a pressure impulse which is measured by a far field microphone array. This calibration source is shown to have its advantages over traditional speakers in that it is non-intrusive (removing additive flow-noise of a body in the flow) and is an impulse (allowing reflections to be removed if desired). Using a set of frequency response functions of the gated signals, the wall transmission loss and the effects of the Kevlar boundary layer are found. The transmission loss is negligible at low frequencies, but increases to 3 dB at 20 kHz and is in good agreement with acoustic theory. The effect of the boundary layer is shown to not exceed 1 dB for the range of frequencies considered. While the transmission loss found herein can be extrapolated to other facilities if the same material is used (assuming linear tension values are similar), the boundary layer effect is likely very dependent on the facility characteristics.

References

[1] Devenport, W., Burdisso, R., Borgoltz, A., Ravetta, P., Barone, M., Brown, K. and Morton, M. The kevlar-walled anechoic wind tunnel, *Journal of Sound and Vibration*, **332**, 3971–3991, (2013).

[2] Jaeger, S., Horne, W. and Allen, C. Effect of surface treatment on array microphone self-noise, (2000).

[3] Burnside, N. J., Horne, W. C., Elmer, K. R., Cheng, R. and Brusniak, L. Phased acoustic array measurements of a 5.75% hybrid wing body aircraft, *54th AIAA Aerospace Sciences Meeting*, p. 0012, (2016).

[4] Ito, T., et al. Aerodynamic/aeroacoustic testing in anechoic closed test ssections of low-speed wind tunnels, (2010).

[5] Ura, H., Yokokawa, Y., Imamura, T., Ito, T. and Yamamoto, K. Airframe noise measurements by using a simplified high-lift model, *27th International Congress of the Aeronautical Sciences*, (2010).

[6] Bahr, C. J., Zawodny, N. S., Bertolucci, B., Li, J., Sheplak, M. and Cattafesta, L. N. A plasma-based non-intrusive point source for acoustic beamforming applications, *Journal of Sound and Vibration*, **344**, 59 – 80, (2015).

[7] Pascioni, K., Reger, R., Edstrand, A. and Cattafesta, L. Characterization of an aeroacoustic wind tunnel facility, 43^{rd} *International Congress on Noise Control Engineering*, (2014).

[8] Underbrink, J., *Practical Considerations in Focused Array Design for Passive Broad-Band Source Mapping Applications*, Master's thesis, Pennsylvania State University, (1995).

[9] Pascioni, K., *An Aeroacoustic Characterization of a Multi-Element High-Lift Airfoil*, PhD dissertation, Florida State University, (2017).

[10] Amiet, R. Refraction of sound by a shear layer, *Journal of Sound and Vibration*, **58**, 467–482, (1978).

[11] Blackstock, D., *Fundamentals of Physical Acoustics*, John Wiley & Sons, Inc. (2000).

[12] Bahr, C., Zawodny, N., Yardibi, T., Liu, F., Wetzel, D., Bertolucci, B. and Cattafesta, L. Shear layer time-delay correction using a non-intrusive acoustic point source, *International Journal of Aeroacoustics*, **10** (5), 497–530, (2011).